Acta Crystallographica Section D
Biological Crystallography
ISSN 0907-4449

Purification, crystallization and preliminary crystallographic studies of a two fibronectin type-III domain segment from chicken tenascin encompassing the heparin- and contactin-binding regions

Daniel Bisig, Peter Weber, Lloyd Vaughan, Kaspar H. Winterhalter and Klaus Piontek*

Laboratorium für Biochemie I, Swiss Federal Institute of Technology (ETH), CH-8092 Zürich, Switzerland

Correspondence e-mail: klaus.piontek@bc.biol.ethz.ch

Received 29 September 1998
Accepted 16 February 1999

A fragment of chicken tenascin consisting of fibronectin type-III domains 5 and 6 has been expressed in *Escherichia coli*. After modifying a previously reported purification protocol, an electrophoretically homogeneous recombinant protein was obtained from which various crystal forms could be grown under identical conditions. Only one form was suitable for structure determination. These crystals belong to space group $P2_1$, with unit-cell parameters $a = 45.2$, $b = 57.9$, $c = 72.2$ Å, $\beta = 91.4^\circ$, and diffract to at least 2.6 Å resolution using synchrotron radiation. From density measurements of the crystals, it was found that there are two molecules in the asymmetric unit. Diffraction data of native, two platinum-derivative and one palladium-derivative crystals were collected.

1. Introduction

Tenascin (TN) is a large multidomain extracellular matrix glycoprotein which exhibits a dynamic spatial and temporal expression both during embryogenesis and in adult tissues (Mackie, 1997). By interaction with various protein and glycosaminoglycan ligands, tenascin-C is thought to mediate diverse biological events such as neural pattern formation, wound healing and carcinogenesis (Vaughan, Zisch *et al.*, 1994; Schnyder *et al.*, 1997).

A characteristic feature of tenascin-C is its large polypeptide chains, which are joined together at the amino termini to generate oligomers which show up as typical 'arms' in electron micrographs (Erickson & Iglesias, 1984; Vaughan *et al.*, 1987). These arms consist of a series of independently folding tandem domains, homologous to epidermal growth factor, fibronectin type-III repeats (fn) and fibrinogen (Spring *et al.*, 1989; Jones *et al.*, 1989; Chiquet-Ehrismann *et al.*, 1994). Similar domains are common to a wide range of molecules involved in cell adhesion and cell signalling. The TNfn regions of tenascin-C can be subdivided into one 'variable' and two 'constant' blocks, the latter two comprising TNfn1–5 and TNfn6–8. Between TNfn5 and TNfn6, up to eight additional fn domains can be spliced in. As tenascin-C forms homo-oligomers (Kaplony *et al.*, 1991), alternative splicing provides the only mechanism for the introduction of new functional elements, apart from post-translational modifications. Identified ligands bind to sites located within the blocks and a few bind to sites spanning two blocks. Of particular biological interest are TNfn domains 5 and 6 of chicken tenascin-C. In the smallest isoform (190 kDa) they are adjacent to each other, enabling binding of the neural cell receptor contactin/F11 (Zisch *et al.*, 1992) and fibronectin (Chiquet-Ehrismann *et al.*, 1991). Contactin is a member of the immunoglobulin superfamily and is thought to play a role in neurite fasciculation. In addition, TNfn5 interacts with the glycosaminoglycan heparan sulfate, which is known to mediate cell attachment (Weber *et al.*, 1995). It forms part of various proteoglycans present on cell surfaces and in the extracellular matrix. *In vitro* experiments show heparin inhibits the interaction between tenascin and contactin/F11 (Weber *et al.*, 1996). To characterize these interactions fully, it is first necessary to elucidate the molecular structures of individual fn domains and their organization within the molecule as a whole.

It is still not understood how the interactions between tenascin-C and its ligands contribute to pattern formation during embryonic development. As a step towards a molecular appreciation of these processes, we attempted to characterize the crystal structure of TNfn56, the domain organization found in the non-alternatively spliced form ('null' isoform) of tenascin, and the binding site for three known ligands. This will permit an analysis of the structural determinants regulating ligand interactions (Jones *et al.*, 1989; Vaughan, Weber *et al.*, 1994; Weber *et al.*, 1996).

2. Materials, results and discussion

2.1. Protein expression and purification

TNfn56 was expressed as a His-tagged fusion protein in *E. coli* M15 cells using the vectors pDS9/56 and PREP4 (Weber *et al.*, 1995). PREP4 mediates kanamycin resistance and encodes for the *lac* repressor protein. pDS9/56 contains a sequence for ampicillin resistance and a sequence of six histidines, followed by a sequence encoding fn domains 5 and 6 of chicken tenascin, a synthetic ribosome-binding site and an optimized lac promoter.

Bacteria were grown in 2YT medium on a rotary shaker. Expression of the fusion protein was induced by addition of isopropyl-β-D-thiogalactopyranoside to a final concentration of 2 m*M*. After 5 h, bacteria were harvested by centrifugation. Cells were disrupted by sonification and insoluble cell debris was separated from soluble compounds. Supernatant was loaded onto an Ni-NTA column (Qiagen) equilibrated with 67 m*M* sodium phosphate, 300 m*M* NaCl, 0.02% NaN_3, pH 8.0. Following several washing steps, the fusion protein was eluted with 100 m*M* sodium acetate (pH 3.8) containing 300 m*M* NaCl and 0.02% NaN_3. Since the fusion protein containing its histidine tag could not be crystallized, the tag was removed by factor Xa cleavage. Complete digestion was achieved by adding 2 µg of factor Xa per milligram of TNfn56 in 20 m*M* Tris–HCl (pH 8.0), 100 m*M* NaCl, 2 m*M* $CaCl_2$ and 0.02% NaN_3 and incubating for 6 h at 310 K and 100 rev min^{-1} on a rotary shaker.

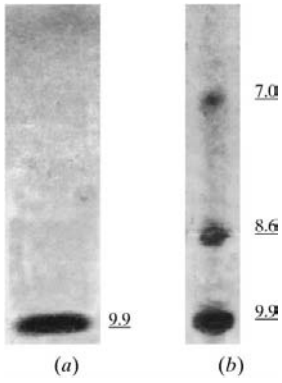

Figure 1
Analytical IEF gels of TNfn56. (*a*) This corresponds to protein which has been purified by cation-exchange chromatography. (*b*) This is a gel where the protein sample was used purified according to the original protocol. The isoelectric point of each protein band is indicated.

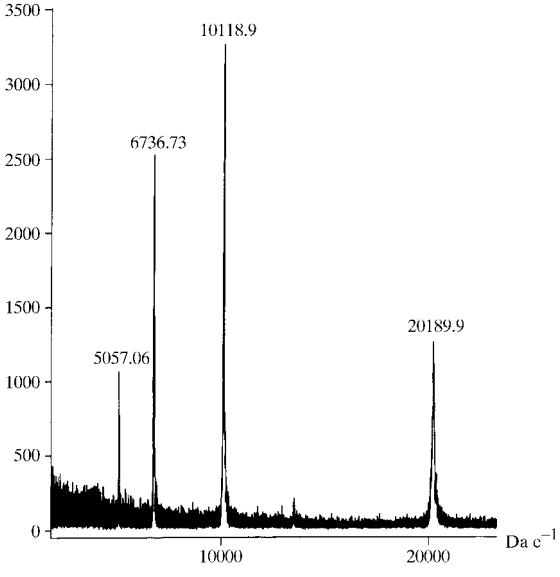

Figure 2
MALDI mass spectrum of TNfn56. The mass labels correspond to the M^+, M^{2+}, M^{3+} and M^{4+} molecular ions. The deviations from the theoretical mass are about 0.2%.

According to the original purification protocol (Weber *et al.*, 1995), the digestion solution was applied to an Ni-NTA column to bind the cleaved histidine tags and the flow-through was applied to a heparin–Sepharose column (Pharmacia) to bind the fusion protein. To remove factor Xa, the heparin–Sepharose column was washed with three column volumes of TBS buffer 1 (10 m*M* Tris–HCl, 20 m*M* NaCl, 0.02% NaN_3, pH 7.5) and the processed TNfn56 was eluted with TBS buffer 2 (10 m*M* Tris–HCl, 1 *M* NaCl, 0.02% NaN_3, pH 7.5).

Protein obtained according to this purification scheme appeared homogeneous by SDS–PAGE and subsequent silver staining. However, several protein bands were readily apparent on isoelectric focusing (IEF) gels (Fig. 1*b*). The major band appears at a p*I* of 9.9, which is in agreement with the theoretical value derived from the amino-acid sequence. Contaminants could be removed by replacing the heparin–Sepharose purification step by cation-exchange chromatography on a Mono-S HR5/5 column (Pharmacia LKB). Typically, 10 mg of TNfn56 was applied to the column in 50 m*M* acetate buffer (pH 4.5) and eluted by a stepwise NaCl gradient. The major protein peak appeared at 300 m*M* NaCl. This protein fraction was judged to be pure, based on analysis by denaturing and native IEF gels (Fig. 1*a*), reverse-phase HPLC and MALDI-MS (Fig. 2).

The cause of the charge heterogeneity of the protein is still unknown. The same heterogenity was found in different IEF gels containing either ampholytes or immobilized pH gradients submerged under silicon oil. Therefore, electrophoretic artefacts can be excluded as causing the multiple bands. Furthermore, since the same pattern can be observed under denaturing conditions, it must be the result of covalent modifications rather than conformational differences. These modifications result only in small molecular-weight differences, since they were not detectable by SDS–PAGE and MALDI-MS. A very common source of non-enzymatic protein modification which results in large charge differences but which barely affects protein size is deamidation (Johnson & Aswad, 1995). The amino-acid sequence –Asn–Ser–, which is particularly prone to deamidation, is present once in TNfn56. In addition, high ionic strength conditions, as applied during elution of TNfn56 from Ni-NTA, heparin and mono-S columns, may increase the rate of deamidation.

2.2. Crystallization, crystal characterization and preparation of heavy-atom derivatives

Crystallization experiments were performed by vapour diffusion using hanging-drop or sitting-drop techniques (McPherson, 1982). Crystals were obtained under various conditions from protein samples purified with the original procedure. However, none of these crystals diffracted beyond a resolution of 5 Å. Since several bands were visible in an analytical IEF gel, the limited resolution was attributed to the inhomogeneity of the protein samples. We therefore developed a purification procedure which yielded electrophoretically pure fusion protein (see above). Further crystallization trials were performed with the pure protein samples obtained by the new purification procedure. Protein of this quality crystallized at room temperature and at 277 K under several conditions of the fast screening kit I (Hampton Research) containing PEG of different molecular weights as precipitant. By refining the crystallization dimensions, a condition (12 mg ml^{-1} protein, 27% PEG 2000, 100 m*M* NaAc pH 4.5) was found which led to growth of elongated wedge-shaped crystals (Fig. 3*a*) within 4–7 d. Many of the crystals were twinned and intergrown or exhibited surfaces disfigured by notches. In addition, they were very sensitive to

Table 1
Characteristics of various TNfn56 crystals.

W1 and W2 correspond to two different forms of wedge-shaped crystals. P400 stands for crystals grown in presence of 4% PEG 400. P represents plate-like crystals. See text for explanation of crystal forms.

Crystal	W1	W2	P400	P
Space group	$P2_1$	$P2_1$	$P2_1$	$P2_1$
a (Å)	48.7	46.5	47.9	45.2
b (Å)	55.2	58.1	55.5	57.9
c (Å)	98.5	72.0	98.1	72.2
β (°)	104.2	91.5	104.4	91.4
Molecules per a.u.	2	2	2	2
Unit-cell volume (Å^3)	256701	194452	252601	187064
V_M (Å^3 Da^{-1})	3.17	2.40	3.12	2.31
Solvent content (%)	61.2	48.8	60.6	46.7
Diffraction limit (Å)	2.8	3.2	3.0	2.55

mechanical and thermal stress. When exposed to X-rays, they scattered to about 3 Å resolution or lower, but unfortunately suffered radiation damage within a few hours. Reduction of precipitant concentrations and addition of 4% PEG 400 led to crystals of improved morphology (Fig. 3*b*) and reduced sensitivity to mechanical and thermal stress. However, these crystals still suffered noticeable radiation damage within a few hours. Other improvements in crystallization strategies, such as reduction of the crystal solvent content by exploiting the water-withdrawing properties of medium and high molecular weight PEG (Schick & Jurnak, 1994) or stabilization of protein conformation by addition of various polyols (Pechik *et al.*, 1993; Sousa *et al.*, 1991; Sousa, 1995), did not improve the crystal properties. Occasionally, plate-like crystals (Fig. 3*c*) appeared within 2–3 weeks under the crystallization conditions which normally give rise to wedge-shaped crystals. These plate-like crystals were of improved stability, exhibited reduced susceptibility to radiation damage and diffracted to at least 2.8 Å resolution. Unfortunately, these crystals could not be obtained directly either by *de novo* crystallization or by various seeding techniques. The addition of small amounts of divalent cations optimized crystallization conditions (12 mg ml^{-1} protein, 27% PEG 2000, 100 m*M* NaAc pH 4.5/5.0, 50–100 m*M* $MgCl_2/CaCl_2$). Under these conditions, seeding techniques were at least partly successful and enabled us to obtain sufficient numbers of crystals. In addition, these crystals were of improved stability and the diffraction limit extended to about 2.6 Å resolution. Experiments to attempt to increase the lifespan of the crystals by cooling them to cryogenic temperature and therefore make more use of the limited number of crystals were not possible, as no in-house facility was available.

The unit-cell dimensions and space group were initially determined based on precession photographs. Improved stability towards radiation damage was achieved by cooling the crystals to 277 K. It was found that all crystal forms belong to space group $P2_1$ (Table 1). Based on unit-cell dimensions, crystals of TNfn56 could be divided into two groups, which mainly differ in the size of the *c* axis and the monoclinic angle, concomitantly leading to different solvent contents. Crystals of lower solvent content diffracted to higher resolution and showed reduced radiation damage. For wedge-shaped crystals, which were obtained most abundantly, the crystal density was determined by suspending them in a Ficoll 400 density gradient. This experiment was necessary in order to exclude the possibility that only one molecule is present per asymmetric unit (a.u.). The experimentally derived V_M value of 2.36 Å^3 Da^{-1} was in good agreement with the V_M value of 2.40 Å^3 Da^{-1} calculated (Matthews, 1968) assuming there to be two molecules in the asymmetric unit (Table 1).

Preparation of heavy-atom derivative crystals has focused on plate-like crystals, owing to their superior stability and diffraction quality compared with wedge-shaped and PEG 400 crystals. However, heavy-atom screening was severely impaired by the limited yield of these crystals. To overcome this problem, early screening experiments involved only the more abundant wedge-shaped crystals, which possess similar cell parameters to the plate-like crystals. Soaking conditions, which did not affect the stability and packing of wedge-shaped crystals, were subsequently applied to the plate-like crystals. Using this approach, three promising derivatives were obtained (Table 2).

2.3. Data collection and processing

Diffraction data of TNfn56 crystals were collected at 277 K using synchrotron radiation (Table 2). Problems during data collection arose from the fact that most crystals suffered severe radiation damage. In addition, non-isomorphism between PEG 400 crystals made it difficult to obtain a complete data set, since many partial data sets had to be discarded. Finally, three partial data sets could be processed and merged together to give acceptable statistics (Table 2). If cryo-conditions could have been used, a single crystal would probably have been sufficient for the collection of a complete data set. However, as mentioned previously, cryo-conditions could not be established owing to the lack of an in-house facility.

An initial data set from plate-like crystals diffracting to 2.8 Å resolution was collected on the EMBL Outstation beamline X31 at the DESY synchrotron, Hamburg using only one crystal. In addition, a second data set containing reflections to 2.55 Å resolution was collected on the Swiss–Norwegian beamline at the ESRF synchrotron, Grenoble, again only with one crystal. The two data sets were processed and merged together, resulting in a statistically reliable data set (Table 2). All heavy-atom derivative data sets of plate-like crystals were obtained with one crystal each on the Swiss–Norwegian beamline and show good internal scaling *R* factors (Table 2).

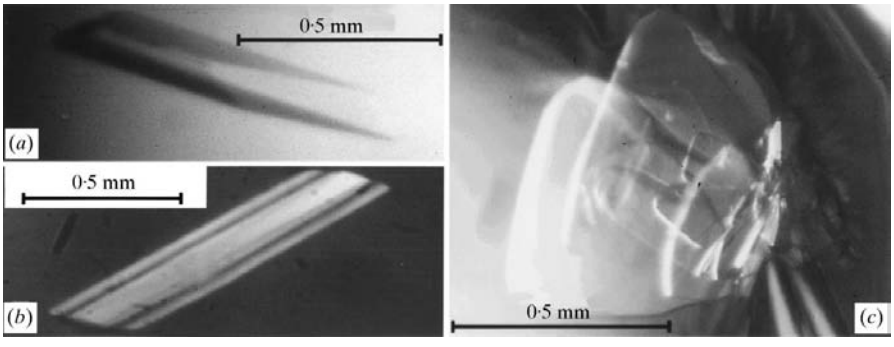

Figure 3
Different crystals of TNfn56. Letters refer to the following crystal types: (*a*) wedge-shaped crystals, (*b*) crystals grown in the presence of 4% PEG 400, (*c*) plate-like crystals.

Table 2
Data collection and processing.

For the meaning of P and P400 see Table 1. Values in parentheses correspond to the highest resolution shell.

Crystal	P400	P	P	P	P
Heavy atom	—	—	K_2PtCl_4	K_2PtCl_4	K_2PdCl_4
Concentration (m*M*)	—	—	1	10	1
X-ray source	DESY synchrotron	DESY/ESRF synchrotron	ESRF synchrotron	ESRF synchrotron	ESRF synchrotron
Detector	MAR Research image plate	MAR Research image plate	MAR Research image plate	MAR Research image plate	MAR Research image plate
Wavelength (Å)	1.01	0.95/0.87	0.87	0.87	0.87
Number of crystals	3	2	1	1	1
Resolution (Å)	16.0–2.9	20.0–2.55	20.0–3.5	15.0–3.2	20.0–2.85
Total number of reflections	41082	68031	17036	27295	39783
Number of unique reflections	10856	11344	4401	5086	8524
Completeness (%)	99.0 (98.2)	93.7 (75.5)	88.5 (87.6)	81.5 (80.3)	98.7 (95.7)
I/σ	6.6 (1.9)	12.7 (2.4)	7.4 (3.8)	9.1 (2.4)	26.4 (7.5)
R_{merge}† (%)	14.5	7.4	10.2	8.0	2.9
R_{iso}‡ (%)	—	—	26.6	17.3	34.5

† $R_{merge} = \sum_h \sum_i |I(h,i) - \langle I(h)\rangle| / \sum_h \sum_i I(h,i)$, where $I(h,i)$ is the intensity of the ith measurement of reflection h and $\langle I(h)\rangle$ is the mean value of $I(h)$ for all i measurements. ‡ $R_{iso} = \sum |F_{PH} - F_P| / \sum F_{PH}$, where F_{PH} and F_P are the derivative and the native structure-factor amplitudes, respectively.

Table 3
Sequence comparison of domains 5 and 6 of TNfn56 with the search models used in molecular replacement.

Sequence identity between domains 5 and 6 of TNfn56 is 30.8%.

Protein	PDB accession code	Residue range used	Identity of amino acids (%)	
			TNfn5	TNfn6
Drosophila neuroglian	1cfb	611–709 (chain *A*)	18.5	27.1
Drosophila neuroglian	1cfb	710–813 (chain *B*)	28.6	32.9
Human fibronectin	1fna	6–96	39.3	41.7
Human fibronectin	1fnf	1143–1235 (chain *A*)	27.8	34.5
Human fibronectin	1fnf	1236–1326 (chain *B*)	33.3	36.0
Human fibronectin	1fnf	1327–1416 (chain *C*)	37.9	40.4
Human fibronectin	1fnf	1418–1509 (chain *D*)	41.2	39.1
Human fibronectin	1ttg	1–94	40.2	37.5
Human tenascin	1ten	803–891	32.2	25.3

Data were processed and scaled with the program package *HKL* (Otwinowski & Minor, 1997). Intensities were converted to structure factors by the use of the program *TRUNCATE* (French & Wilson, 1978) from the *CCP*4 (Collaborative Computational Project, Number 4, 1994) suite of programs.

2.4. Molecular replacement and MIR phasing

The structure determination was attempted by molecular and isomorphous replacement techniques in parallel. In an initial step towards molecular replacement, we intended to determine the relation between the two crystallographically independent molecules in the asymmetric unit (a.u.). Since this non-crystallographic symmetry did not necessarily have to be that of a point group (*e.g.* *C*2), general self-rotation functions had to be calculated. Numerous self-rotation functions were calculated with the programs *AMoRe* (Navaza, 1994), *X-PLOR* (Brünger, 1993; DeLano & Brünger, 1995) and *GLRF* (Tong & Rossmann, 1997), but no prominent peak was found apart from the maximum related to the crystallographic 2_1 axis. To test whether a possible non-crystallographic twofold axis was parallel to or inclined by only a small angle to the crystallographic axis and therefore hidden under the maximum from the crystallographic axis, the Harker section of a native Patterson map was inspected. No significant peak was found and it was concluded that the intermolecular rotation does not have twofold symmetry. The interpretation of the self-rotation function was further complicated by the fact that each TNfn56 molecule has an internal pseudo-symmetry, as domains 5 and 6 have the same fold. From related multiple fn-domain structures (Leahy *et al.*, 1996; Muller *et al.*, 1996; Huber *et al.*, 1994), it is known that the rotation between two domains can vary between about 40° and about 170°. Despite much effort, identification of the non-crystallographic symmetry with self-rotation functions was not possible, and we proceeded with cross-rotation functions using several search models consisting of single fn domains which were obtained from the Protein Data Bank (Abola *et al.*, 1987). The molecular-replacement approach involved a four-body problem, which is not trivial if no good search model is available. The search models used have only low sequence homology with either domain 5 or 6 of TNfn56 (Table 3). Despite significant peaks being found in the cross-rotation functions, these possible solutions, in combination with the lack of prominent peaks in the translation functions, did not allow us to obtain an unambiguous solution for the four fn modules in the asymmetric unit. These results point to large structural differences, a reflection of the small sequence identities between the search models and the two domains of TNfn56.

The scaling *R* factor of the heavy-atom derivative data to the native data indicate that the crystals have been successfully derivatized (Table 2). However, inspection of Harker sections in difference Patterson maps showed that the derivative data contain many sites and no major site(s) which could be used for initial phasing and subsequent application of difference Fourier techniques. Attempts to refine the heavy-atom positions as well as a search for a single and/or a major heavy-atom site derivative is currently in progress. It is planned to improve the initial MIR phases by real-space averaging about the two TNfn56 molecules in the crystallographic asymmetric unit, eventually including averaging between the two crystal forms.

We gratefully acknowledge the opportunity to collect diffraction data at the EMBL Outstation, DESY, Hamburg, Germany and on the Swiss–Norwegian beamline at the ESRF, Grenoble, France. We thank Zsbyszek Dauter and Wojtek Rypniewski, EMBL Outstation, Hamburg, for support during data collection. This work was funded by an ETH research grant (0-20-748-93) to KP. Dr Lucia Rohrer is thanked for fruitful discussions regarding protein purification.

References

Abola, E. E., Bernstein, F. C., Bryant, S. H., Koetzle, T. F. & Weng, J. (1987). *Crystallographic Databases – Information Content, Software Systems, Scientific Applications*, edited by F. H. Allen, G. Bergerhoff & R. Sievers, pp. 107–132. Bonn/Cambridge/Chester: IUCr.

Brünger, A. T. (1993). *X-PLOR Version 3.1 Manual.* New Haven: Yale University Press.
Chiquet-Ehrismann, R., Matsuoka, Y., Hofer, U., Spring, J., Bernasconi, C. & Chiquet, M. (1991). *J. Cell Biol.* **127**, 2093–2101.
Chiquet-Ehrismann, R., Tannheimer, M., Koch, M., Brunner, A., Spring, J., Martin, D., Baumgartner, S. & Chiquet, M. (1994). *Cell Regul.* **2**, 927–938.
Collaborative Computational Project, Number 4 (1994). *Acta Cryst.* D**50**, 760–763.
DeLano, W. L. & Brünger, A. T. (1995). *Acta Cryst.* D**51**, 740–748.
Erickson, H. P. & Iglesias, J. L. (1984). *Nature (London)*, **311**, 267–269.
French, S. & Wilson, K. (1978). *Acta Cryst.* A**34**, 517–525.
Huber, A. H., Wang, Y.-M. E., Bieber, A. J. & Bjorkman, P. J. (1994). *Neuron*, **12**, 717–731.
Johnson, B. A. & Aswad, D. W. (1995). *Deamidation and Isoaspartate Formation in Peptides and Proteins*, edited by D. W. Aswad, pp. 91–113. Boca Raton: CRC Press.
Jones, F. S., Hoffman, S., Cunningham, B. A. & Edelmann, G. M. (1989). *Proc. Natl Acad. Sci. USA*, **86**, 1905–1909.
Kaplony, A., Zimmermann, D. R., Fischer, R. W., Imhof, B. A., Odermatt, B. F., Winterhalter, K. H. & Vaughan, L. (1991). *Development*, **112**, 605–614.
Leahy, D. J., Aukhil, I. & Erickson, H. P. (1996). *Cell*, **84**, 155–164.
Mackie, E. J. (1997). *J. Biochem. Cell Biol.* **29**, 1133–1137.
McPherson, A. (1982). *Preparation and Analysis of Protein Crystals.* New York: John Wiley & Sons.
Matthews, B. W. (1968). *J. Mol. Biol.* **33**, 491–497.
Muller, Y. A., Ultsch, M. H. & de Vos, A. M. (1996). *J. Mol. Biol.* **256**, 144–159.
Navaza, J. (1994). *Acta Cryst.* A**50**, 157–163.
Otwinowski, Z. & Minor, W. (1997). *Methods Enzymol.* **276**, 307–326.
Pechik, I., Nachman, J., Ingham, K. & Gilliland, G. L. (1993). *Proteins*, **16**, 43–47.
Schick, B. & Jurnak, F. (1994). *Acta Cryst.* D**50**, 563–568.
Schnyder, B., Semadeni, R. O., Fischer, R. W., Vaughan, L., Car, B. D., Heitz, P. U., Winterhalter, K. H. & Odermatt, B. F. (1997). *Int. J. Cancer*, **72**, 217–224.
Sousa, R. (1995). *Acta Cryst.* D**51**, 271–277.
Sousa, R., Lafer, E. M. & Wang, B. C. (1991). *J. Cryst. Growth*, **110**, 237–246.
Spring, J., Beck, K. & Chiquet-Ehrismann, R. (1989). *Cell*, **59**, 325–334.
Tong, L. & Rossmann, M. G. (1997). *Methods Enzymol.* **276**, 594–611.
Vaughan, L., Huber, S., Chiquet, M. & Winterhalter, K. H. (1987). *EMBO J.* **6**, 349–353.
Vaughan, L., Weber, P., D'Alessandri, L., Zisch, A. H. & Winterhalter, K. H. (1994). *Perspect. Dev. Neurobiol.* **2**, 43–52.
Vaughan, L., Zisch, A. H., Weber P., D'Allesandri, L., Ferber, P., David, G., Zimmermann, D. R. & Winterhalter, K. H. (1994). *Contrib. Nephrol.* **107**, 80–84.
Weber, P., Ferber, P., Fischer, R., Winterhalter, K. H. & Vaughan, L. (1996). *FEBS Lett.* **389**, 304–308.
Weber, P., Zimmermann, D. R., Winterhalter, K. H. & Vaughan, L. (1995). *J. Biol. Chem.* **270**, 4619–4623.
Zisch, A. H., D'Alessandri, L., Rantsch, B., Falchetto, R., Winterhalter, K. H. & Vaughan,, L. (1992). *J. Cell Biol.* **119**, 203–213.